PHYSICAL REVIEW B **92**, 241405(R) (2015)

Intermolecular artifacts in probe microscope images of C_{60} assemblies

Samuel Paul Jarvis,* Mohammad Abdur Rashid, Adam Sweetman, Jeremy Leaf, Simon Taylor, Philip Moriarty,† and Janette Dunn

School of Physics & Astronomy, University of Nottingham, Nottingham, NG7 2RD, United Kingdom

(Received 4 September 2015; revised manuscript received 16 October 2015; published 9 December 2015)

Claims that dynamic force microscopy has the capability to resolve intermolecular bonds in real space continue to be vigorously debated. To date, studies have been restricted to planar molecular assemblies with small separations between neighboring molecules. Here we report the observation of intermolecular artifacts over much larger distances in 2D assemblies of C_{60} molecules, with compelling evidence that in our case the tip apex is terminated by a C_{60} molecule (rather than the CO termination typically exploited in ultrahigh resolution force microscopy). The complete absence of directional interactions such as hydrogen or halogen bonding, the nonplanar structure of C_{60}, and the fullerene termination of the tip apex in our case highlight that intermolecular artifacts are ubiquitous in dynamic force microscopy.

DOI: 10.1103/PhysRevB.92.241405 PACS number(s): 68.37.Ps, 68.37.−d

I. INTRODUCTION

Intermolecular interactions are fundamental in nature, governing the chemistry "beyond the molecule" [1,2] responsible for stabilizing self-assembled arrays of molecules and supramolecular systems. The potential to investigate intermolecular interactions at the single bond limit is therefore particularly attractive. As such, scanning probe microscopy has especially promising potential for the investigation of molecular and supramolecular self-assembly at surfaces [3–5]. In a few short years, dynamic force microscopy [also called noncontact atomic force microscopy (NC-AFM)] has provided unprecedented submolecular detail at the single bond level for a variety of systems [6–13]. This has been achieved by terminating the scanning probe with a single molecule [14,15] or *via* spontaneous termination of the tip apex [16–19], which is subsequently moved so close to the underlying molecule that repulsive tip-sample interactions from the molecular skeleton yield exceptionally high resolution.

In addition to resolving the internal structure of a molecule, NC-AFM and the scanning tunneling hydrogen microscopy (STHM) method pioneered by Termirov and co-workers [20] have both shown that apparent intermolecular features can be resolved in molecular assemblies, stabilized either through hydrogen bonds [18,21–23] or, very recently, halogen-bonding interactions [24]. Although initial density functional theory (DFT) modeling of the tip-sample interaction in hydrogen bonded assemblies showed good agreement with experimental line profile measurements above inter- and intramolecular features, it failed to reproduce the striking appearance observed in experiment [18], where the bonds appeared much sharper. Subsequently, several studies have now shown that tip flexibility [25–27], especially at very close tip-sample separations, is responsible for the striking intra- and intermolecular resolution observed with various SPM techniques [22,27,28] and that apparent intermolecular features can be observed with NC-AFM even when no bonding interaction is present [23], suggesting that the features are, in fact, an artifact and cannot be interpreted as a real-space image of an intermolecular bond. Aspects of this interpretation have, however, in turn been challenged very recently [29].

In each of the reported cases where intermolecular resolution has thus far been observed, the molecules under study have all been planar in structure and generally stabilized through hydrogen bonding interactions with interatomic separations below the sum of the vdW radii. Here we show that apparent intermolecular features can also be observed over much larger distances in two-dimensional assemblies of C_{60} molecules that are neither planar in structure nor stabilized through any other intermolecular bonding mechanism beyond van der Waals forces. By modeling the tip-sample interaction using a variant of the simple Lennard-Jones models introduced in earlier work [22,23,27], we show that a C_{60}-terminated tip which is free to move on the end of the force microscope probe can account for the intermolecular features observed experimentally. As the intermolecular interactions in C_{60} islands arise solely from dispersion forces, it is clear that entirely artifactual contrast between molecules can arise even for systems which are nonplanar and where the apex of the tip of the force microscope is not terminated with a CO molecule. This has significant implications for the interpretation of high resolution force microscope images.

II. METHODS

Experimental measurements were obtained on different sample substrates using two commercial scanning probe instruments. Measurements with C_{60} deposited on Cu(111) and NaCl:Cu(111) surfaces were obtained using a Createc GmbH LT STM-AFM system operating at liquid helium temperatures (∼5 K), while results on Ag:Si(111)-($\sqrt{3} \times \sqrt{3}$) and multilayer C_{60} on Si(111) were obtained using an Omicron Nanotechnology GmbH LT STM-AFM system operating at liquid nitrogen temperatures (∼77 K). We also studied assemblies of the endofullerene molecule, $H_2O@C_{60}$,

*samuel.jarvis@nottingham.ac.uk
†philip.moriarty@nottingham.ac.uk

which were deposited using the same thermal evaporation procedure as used for the empty C_{60} cages. (We stress that the $H_2O@C_{60}$ endofullerene is indistinguishable—both as an isolated molecule and in images of molecular islands—from the empty C_{60} cage in STM images, NC-AFM images, and $df(z)$ curves.). Both systems were kept under ultrahigh vacuum conditions with a base pressure $<6 \times 10^{-11}$ mbar or better. The Createc (Omicron) systems were equipped with qPlus sensors [30] using an electrochemically etched tungsten wire attached to one tine of a tuning fork with typical parameters of $f_0 \sim 20$ kHz ($\sim$25 kHz) and $k \sim 1800$ Nm^{-1} ($\sim$2000 Nm^{-1}). Tips were prepared *via* controlled tip crashing and bias voltage pulsing until good STM/NC-AFM resolution was achieved. See the Supplemental Material [31] for details of the sample preparation.

To simulate NC-AFM images, we adapted the flexible tip method as previously reported [22,27] to model the interaction between a sample and either a CO or C_{60}-functionalized probe. We describe the method in detail in the Supplemental Material [31]. The functionalized tip is assumed to consist of a *tip base* (outermost atom of the metal tip) and a *probe particle*. The probe particle is the flexible end of the model tip and is allowed to move around the tip base. The probe particle experiences three forces: (i) due to the tip base, (ii) a sum of all pairwise forces due to interactions with atoms in the sample, and (iii) a lateral harmonic force from the tip base.

In the case of a C_{60}-functionalized tip, we take the C_{60} molecule to act in the same way as a single effective probe particle, similar to the CO tip. The parameters for the "interatomic" (Lennard-Jones) potentials were chosen to take into account that the probe and tip base are not actually single atoms. Therefore, both the tip base and the probe particle were approximated as C_{60} molecules using a radius of $r_\alpha = 5.0$ Å, compared to the values of 2.0 Å and 1.661 Å, respectively, used for CO. For the probe particle, we kept the same value for ϵ_α that was used for a CO-functionalized tip, namely 9.106 meV. However, for the tip base we used a much larger value of the ϵ_α parameter in the Lennard-Jones potential (15 eV), compared to 1 eV in Ref. [22]. For our model, the much higher value of ϵ_α was required to keep the probe particle bound to the tip base while maintaining some flexibility in the z direction. For all simulations a lateral stiffness of $k_{xy} = 0.5$ Nm^{-1} was used for the tip.

III. RESULTS

In Figs. 1(a) and 1(b) we show NC-AFM frequency shift images of islands of $H_2O@C_{60}$ on the Cu(111) surface and C_{60} on a C_{60}-terminated Si(111) surface [i.e., the substrate is a monolayer of C_{60} chemisorbed on Si(111), on which there are physisorbed C_{60} islands], respectively, recorded in the constant height mode at small tip-sample separation. At these distances, repulsive contributions to the tip-sample force dominate the observed contrast resulting in the fullerene molecules appearing brighter (less negative Δf) relative to the vdW background. This results in the clear appearance of the hexagonally packed arrangement of the fullerene molecules with a nearest neighbor separation of $\sim$1 nm. Despite this large separation, in addition to the intramolecular structure observed within the individual fullerenes (see Supplemental Material in Ref. [32], and Refs. [33,34]), clear interconnecting features are observed between each nearest neighbor molecule taking on a similar appearance to previous reports examining hydrogen bonded molecules. This is highlighted in the schematic shown in Fig. 1(d) and the line profile measurement in Fig. 1(c), where, on average, the corrugation due to the molecule itself appears $\sim$3–8 times brighter than the interconnecting features (see Ref. [31] for additional data). That both empty and filled C_{60} cages produce such similar contrast in our images suggests that observations of interconnecting features are general across fullerene molecules.

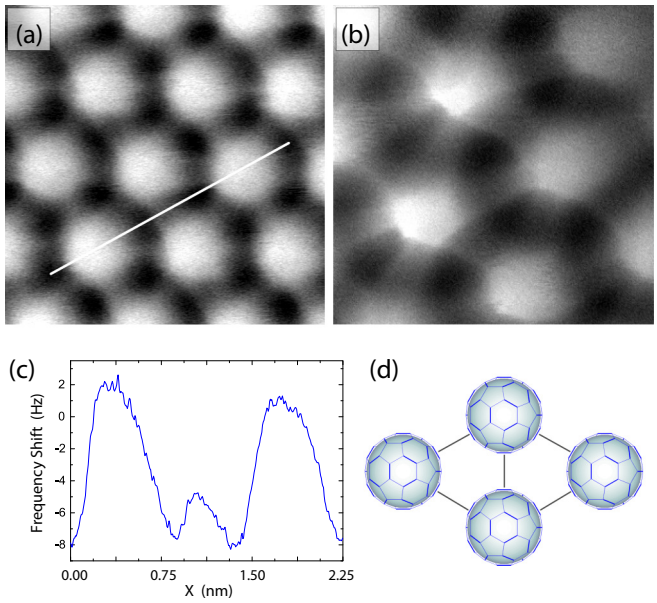

FIG. 1. (Color online) Apparent intermolecular features. NC-AFM frequency shift images of a 2D assembly of (a) a thick (six-layer) film of $H_2O@C_{60}$ and (b) C_{60} molecules recorded in the constant height mode, revealing interconnecting features between nearest neighbor molecules. (c) Line profile measurement along the white line shown in (a). (d) Schematic of the C_{60} packing arrangement and locations of apparent intermolecular features. Parameters: (a) image size: 3.2 nm × 3.2 nm, oscillation amplitude: $a_0 = 300$ pm; (b) image size: 2.3 nm × 2.3 nm, oscillation amplitude: $a_0 = 110$ pm.

In order to better characterize the tip-sample interactions responsible for the artifactual intermolecular contrast, the measurements were repeated at various tip-sample separations. Figures 2(b)–2(e) show a sequence of constant height frequency shift images acquired for a single layer island of C_{60} molecules deposited onto a thin film of NaCl grown on Cu(111), where the tip-sample separation was slowly reduced over the course of several hours. The preceding constant height current image shown in Fig. 2(a) reveals that the island is made up from C_{60} molecules of mixed orientation forming a (2×2) superstructure [35,36]. As the tip-sample distance is reduced, attractive vdW interactions cause the C_{60} molecules to initially appear as dark depressions as shown in Fig. 2(b), corresponding to a more negative frequency shift relative to the background signal. At smaller tip-sample distances, as shown in Fig. 2(c), the emergence of intramolecular structure is observed within each C_{60} molecule due to the onset of repulsive interactions beyond the force interaction turnaround. Finally, at

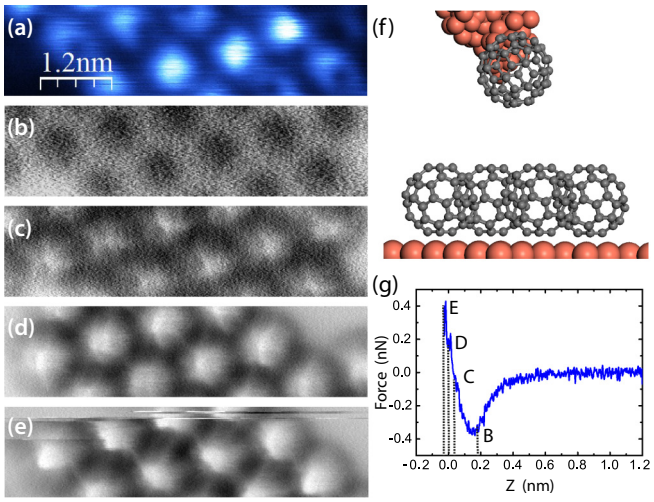

FIG. 2. (Color online) (a) Constant height current image of a C_{60} island prior to NC-AFM measurements (recorded at +500 mV sample bias). (b)–(e) Progression of constant height frequency shift images with decreasing tip-sample separation (recorded at 0 V sample bias and oscillation amplitude: $a_0 = 300$ pm). In (b) the C_{60} molecules appear dark due to attractive vdW interactions; in (c)–(e) the molecules appear bright due to the onset of tip-sample repulsion. Clear apparent intermolecular features are again observed in (e). (f) Illustrative and schematic diagram of experimental setup. Note that we show a single C_{60} molecule bound to the tip apex. It is more likely that the tip apex is covered with a number of C_{60} molecules. (g) Measurement of $F(z)$ recorded above the rightmost surface C_{60} molecule. The peak attractive force of −0.34(6) nN suggests that the NC-AFM tip is C_{60} terminated.

very small tip-sample separations shown in Figs. 2(d) and 2(e), apparent intermolecular features are observed.

Compared to the image shown in Fig. 1(a), the interconnecting features observed in Fig. 2(e) show an asymmetry in their appearance, either appearing as single or two parallel lines, strongly suggestive of an asymmetric tip-sample interaction potential. We note that the appearance and symmetry of the intermolecular features showed no dependence on the underlying sample substrate used to support the C_{60} molecules, which is instead determined by changes in the tip structure. (We return to this point below.) In addition, compared to Figs. 2(c) and 2(d) the *intra*molecular contrast is reduced, to the extent that it is almost no longer observable. This is similar to observations made by Hämäläinen *et al.* [23], who note that at small tip-sample distances tip flexibility can start to "level out" the Δf signal limiting the spatial resolution. The small tip-sample distances necessary to observe the apparent intermolecular features can also result in significant restructuring of C_{60} islands, as observed in the top part of the scan in Fig. 2(e). At larger tip-sample separations, Figs. 2(a)–2(c), the locations of the C_{60} molecules remain unchanged, whereas in Figs. 2(d) and 2(e) the C_{60} molecules at the left and right edges of the island begin to move. This culminates in the complete destruction of the island in the image immediately following Fig. 2(e), as the tip-sample interaction becomes so great that the entire island was swept away (often accompanied by molecules being transferred to the tip). This is consistent with the weak intermolecular interactions within the C_{60} layer.

Although intramolecular features are observed within each C_{60} molecule, the features are not as clear compared to experiments where a well defined CO tip termination revealed the atomic structure of the cage [7], suggesting a more complicated tip-sample convolution. In the experiments described here no deliberate tip functionalization, either with CO or any other small molecule, takes place. We instead expect that the scanning probe is terminated by a C_{60} molecule picked up from the sample surface, either directly onto the metal tip or, more likely, onto a cluster of accumulated C_{60} molecules. From an experimental perspective, this is partly motivated by the relative ease with which the molecular islands can be disturbed during scanning in both STM and NC-AFM modes, where we often observe the disappearance of single C_{60} molecules following controlled $I(z)$ or $F(z)$ measurements, but also the relatively consistent appearance of the molecules on each of the four sample substrates we used (two of which were multilayer C_{60} samples). Moreover, in some instances immediately following measurements on C_{60}, we carried out experiments on a clean Cu(111) substrate (in order to recover the tip) where molecular deposition from the tip onto the surface was repeatedly observed.

Quantitative measurements of the force interaction between two molecules [32,37,38] can also provide insights into the tip termination. For C_{60} in particular, the pair potential between two molecules can be measured [32] and compared to the analytical Girifalco potential [39]. $F(z)$ measurements taken with the same tip as that shown in Fig. 2 show a maximum attractive force ranging from −0.32 nN to −0.36 nN, an example of which is shown in Fig. 2(f). (We stress, however, that there are pitfalls in using "signature" values of maximum intermolecular force/potential energy to characterize the tip apex as different tip apices can often give rise to similar force curves.) Nonetheless, the average maximum attractive force value of 0.34(6) nN [40] is similar to previous reports where we used a C_{60}-terminated tip and also falls within the range expected due to the orientation dependence of each C_{60} molecule [41]. It is also worth noting that Gross *et al.* [42] measure a 100 pN maximum attractive force for a CO molecule interacting with a C_{60} molecule. Consequently, although we cannot eliminate the possibility of alternative tip terminations, it is likely that the contrast we observe is due to a C_{60} molecule terminating the tip apex. The simulations described below provide strong support for this assertion.

In order to interpret our experimental data, and, in particular, to elucidate the origin of the artifactual intermolecular contrast, we simulated constant height NC-AFM images of a C_{60} island using the simple Lennard-Jones model described above using three different tip terminations. In addition to modeling the flexible CO tip used by other groups [22,23,27,28], we also tested both flexible and rigid probe particles using a radius of 5 Å in order to approximate a C_{60}-terminated tip. Simulated images of the tip-sample force resulting from these three tip terminations are shown in Fig. 3 at different tip-sample separations. Whereas the flexible CO-tip model clearly resolves the internal atomic structure of each C_{60} molecule within the island, revealing the hexagonal face at $z = -50$ pm, interconnecting features between the fullerenes

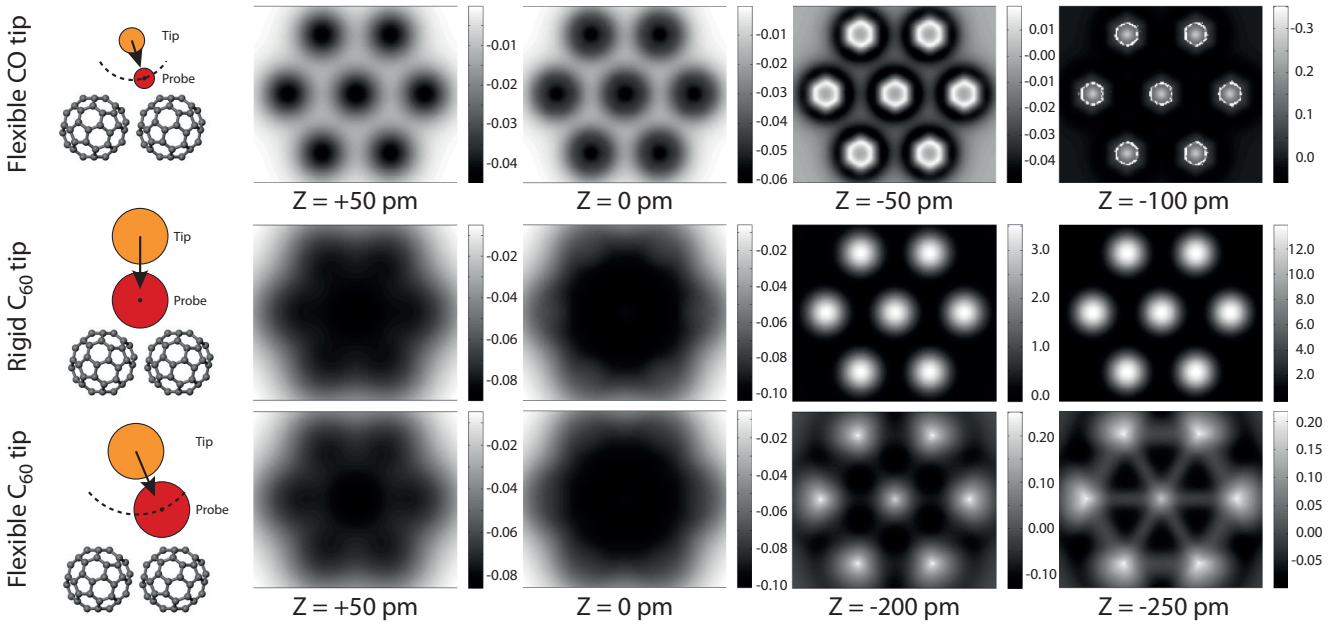

FIG. 3. (Color online) Simulated NC-AFM images using a flexible Lennard-Jones tip model. (Top) Force images of an island of seven hexagon-up orientated C_{60} molecules modeled using a flexible CO probe particle at decreasing tip-sample separations. At $Z = -50$ pm the hexagonal face of the molecules can clearly be observed. Force images of the same island were also modeled using a large radius (5 Å) probe particle representing a C_{60} terminated tip maintained in either a fixed geometry (middle) or allowed to relax (bottom). While internal features can no longer be resolved due to the large probe radius, clear interconnecting features can be seen for the flexible C_{60} tip model. Smaller tip-sample Z heights are shown for the large probe radius tip due to a shallower force profile arising from the choice of Lennard-Jones parameters. The color scale shown in nN for all images.

are absent, even at very small tip-sample distances. Similarly, despite using a much larger probe particle radius, simulations using a *rigid* "C_{60}" probe also fail to resolve interconnecting features. Only when the large radius probe is allowed to relax do clear interconnecting features, akin to those observed in experiment, appear in the simulations.

Just as was found for the experimental images shown in Fig. 2, the interconnecting intermolecular features only become visible in the simulations at tip-sample distances below ~ -200 pm (relative to the force turnaround), past the point at which repulsion is observed within the individual molecules. Surprisingly, even at very small tip-sample separations, interconnecting features are never observed in the fixed C_{60} simulation with the center point between molecules always appearing as the point of minimum force. This is surprising, as one of the important effects of the flexible tip model is usually to "normalize" the intramolecular and intermolecular contributions to the image such that they appear with similar brightness. For instance, at a tip height of $z = -200$ pm the fixed C_{60} simulation reveals forces over an order of magnitude greater over the molecule compared to the flexible tip. This confirms that it is only with the combination of *both* a large radius C_{60} tip *and* the flexible junction (which we attribute to the weakly bound nature of a single C_{60} at the apex of a molecular tip-cluster) that interconnecting features can be observed.

It should also be noted that the simulations do not have periodic boundary conditions in place. Thus, it is only the molecule at the center of the cluster which is associated with a sixfold symmetric potential. The six molecules at the edges of the cluster do not have neighbors, and so the tip-sample interaction potential lacks the same symmetry. The effects of this symmetry-breaking on the images is manifest in two ways. First, the thickness of the intermolecular "bonds" is different between molecules at the edge of the cluster as compared to the features connecting the center molecule to its neighbours. Second, the shapes of the molecules themselves differ. Each of the six molecules at the edge of the cluster has a triangular shape, as compared to the much more circularly-symmetric appearance of the center molecule. As noted above in reference to Fig. 2(e), we also see variations in intermolecular contrast along different crystallographic directions in the experimental NC-AFM images *within* a molecular island. For the experiment, the symmetry is broken not by the surface-adsorbed molecules but by the tip, raising the very intriguing possibility that intermolecular contrast could be exploited to characterize the symmetry of the tip apex.

The success of the flexible tip model, both here and in other papers [22,23,27,28], makes it tempting to ask whether any bond, intermolecular or internal to the molecule, is ever directly imaged in NC-AFM. Even though Lennard-Jones potentials are only a crude approximation of the real electronic density of the molecules, the success of the model suggests that if the overlap of spherical potentials, coupled with the flexibility and finite size of the probe, is sufficient to reproduce the contrast between the atoms, then it is not immediately apparent to what extent the (real) electronic density within a bond contributes to the contrast or whether the experimental

images might also be dominated by the electronic density centered over the atoms.

IV. CONCLUSION

In summary, we report the observation of features appearing as artificial intermolecular bonds in 2D assemblies of C_{60} molecules. Experimental measurements, combined with simulations based on simple analytical potentials, support our view that apparent intermolecular features, in this system, are only visible if the NC-AFM probe is terminated with a flexible C_{60} molecule, capable of relaxing in the tip-sample junction. That intermolecular artifacts are observed in the nonplanar, van der Waals-mediated fullerene system, and only in the presence of a C_{60}, rather than a CO-terminated, tip apex, highlights that artifactual intermolecular contrast is a key issue for ultrahigh resolution force microscopy of a range of molecular systems.

ACKNOWLEDGMENTS

We gratefully acknowledge helpful discussions with Prokop Hapala and Sampsa Hämäläinen regarding the simulation code and Leo Gross for sharing data on force measurements. S.P.J would like to thank the Engineering and Physical Sciences Research Council (EPSRC) and the Leverhulme Trust, respectively, for the award of fellowships EP/J500483/1 and ECF-2015-005. P.J.M. thanks the Engineering and Physical Sciences Research Council (EPSRC) and the Leverhulme Trust, respectively, for Grants No. EP/G007837/1 and No. F00/114 BI. A.S. acknowledges the support of the Leverhulme Trust via fellowship ECF-2013-525. J.L. and S.T. are supported by EPSRC studentship funding. M.A.R. thanks the University of Nottingham for award of a Vice Chancellor's Scholarship for Research Excellence.

[1] J.-M. Lehn, Proc. Natl. Acad. Sci. U.S.A. **99**, 4763 (2002).
[2] J.-M. Lehn, Chem. Soc. Rev. **36**, 151 (2007).
[3] J. A. Theobald, N. S. Oxtoby, M. A. Phillips, N. R. Champness, and P. H. Beton, Nature (London) **424**, 1029 (2003).
[4] L. Grill, M. Dyer, L. Lafferentz, M. Persson, M. V. Peters, and S. Hecht, Nat. Nanotechnol. **2**, 687 (2007).
[5] J. V. Barth, G. Costantini, and K. Kern, Nature (London) **437**, 671 (2005).
[6] L. Gross, F. Mohn, N. Moll, P. Liljeroth, and G. Meyer, Science **325**, 1110 (2009).
[7] L. Gross, F. Mohn, N. Moll, B. Schuler, A. Criado, E. Guitián, D. Peña, A. Gourdon, and G. Meyer, Science **337**, 1326 (2012).
[8] N. Pavliček, B. Fleury, M. Neu, J. Niedenführ, C. Herranz-Lancho, M. Ruben, and J. Repp, Phys. Rev. Lett. **108**, 086101 (2012).
[9] D. G. de Oteyza, P. Gorman, Y.-C. Chen, S. Wickenburg, A. Riss, D. J. Mowbray, G. Etkin, Z. Pedramrazi, H.-Z. Tsai, A. Rubio, M. F. Crommie, and F. R. Fischer, Science **340**, 1434 (2013).
[10] S. P. Jarvis, S. Taylor, J. D. Baran, N. R. Champness, J. A. Larsson, and P. Moriarty, Nat. Commun. **6**, 8338 (2015).
[11] A. M. Sweetman, S. P. Jarvis, P. Rahe, N. R. Champness, L. N. Kantorovich, and P. J. Moriarty, Phys. Rev. B **90**, 165425 (2014).
[12] L. Gross, Nat. Chem. **3**, 273 (2011).
[13] S. P. Jarvis, Int. J. Mol. Sci. **16**, 19936 (2015).
[14] F. Mohn, B. Schuler, L. Gross, and G. Meyer, Appl. Phys. Lett. **102**, 073109 (2013).
[15] G. Kichin, C. Weiss, C. Wagner, F. S. Tautz, and R. Temirov, J. Am. Chem. Soc. **133**, 16847 (2011).
[16] O. Guillermet, S. Gauthier, C. Joachim, P. de Mendoza, T. Lauterbach, and A. Echavarren, Chem. Phys. Lett. **511**, 482 (2011).
[17] S. Kawai, A. Sadeghi, X. Feng, P. Lifen, R. Pawlak, T. Glatzel, A. Willand, A. Orita, J. Otera, S. Goedecker, and E. Meyer, ACS Nano **7**, 9098 (2013).
[18] A. M. Sweetman, S. P. Jarvis, H. Sang, I. Lekkas, P. Rahe, Y. Wang, J. Wang, N. R. Champness, L. Kantorovich, and P. Moriarty, Nat. Commun. **5**, 3931 (2014).
[19] H. Sang, S. P. Jarvis, Z. Zhou, P. Sharp, P. Moriarty, J. Wang, Y. Wang, and L. Kantorovich, Sci. Rep. **4**, 6678 (2014).
[20] R. Temirov, S. Soubatch, O. Neucheva, A. C. Lassise, and F. S. Tautz, New J. Phys. **10**, 053012 (2008).
[21] J. Zhang, P. Chen, B. Yuan, W. Ji, Z. Cheng, and X. Qiu, Science **342**, 611 (2013).
[22] P. Hapala, G. Kichin, C. Wagner, F. S. Tautz, R. Temirov, and P. Jelínek, Phys. Rev. B **90**, 085421 (2014).
[23] S. K. Hämäläinen, N. van der Heijden, J. van der Lit, S. den Hartog, P. Liljeroth, and I. Swart, Phys. Rev. Lett. **113**, 186102 (2014).
[24] S. Kawai, A. Sadeghi, F. Xu, L. Peng, A. Orita, J. Otera, S. Goedecker, and E. Meyer, ACS Nano **9**, 2574 (2015).
[25] N. Moll, B. Schuler, S. Kawai, F. Xu, L. Peng, A. Orita, J. Otera, A. Curioni, M. Neu, J. Repp, G. Meyer, and L. Gross, Nano Lett. **14**, 6127 (2014).
[26] M. Neu, N. Moll, L. Gross, G. Meyer, F. J. Giessibl, and J. Repp, Phys. Rev. B **89**, 205407 (2014).
[27] M. P. Boneschanscher, S. K. Hämäläinen, P. Liljeroth, and I. Swart, ACS Nano **8**, 3006 (2014).
[28] P. Hapala, R. Temirov, F. S. Tautz, and P. Jelínek, Phys. Rev. Lett. **113**, 226101 (2014).
[29] C.-S. Guo, X. Xin, M. A. Van Hove, X. Ren, and Y. Zhao, J. Phys. Chem. C **119**, 14195 (2015).
[30] F. J. Giessibl, Appl. Phys. Lett. **73**, 3956 (1998).
[31] See Supplemental Material at http://link.aps.org/supplemental/10.1103/PhysRevB.92.241405 for full details on the sample preparation, simulation methods, additional experimental images and simulated probe particle trajectories.
[32] C. Chiutu, A. M. Sweetman, A. J. Lakin, A. Stannard, S. Jarvis, L. Kantorovich, J. L. Dunn, and P. Moriarty, Phys. Rev. Lett. **108**, 268302 (2012).
[33] R. Pawlak, S. Kawai, S. Fremy, T. Glatzel, and E. Meyer, ACS Nano **5**, 6349 (2011).
[34] R. Pawlak, S. Kawai, S. Fremy, T. Glatzel, and E. Meyer, J. Phys. Condens. Matter **24**, 084005 (2012).
[35] F. Rossel, M. Pivetta, F. Patthey, E. Ćavar, A. P. Seitsonen, and W. D. Schneider, Phys. Rev. B **84**, 075426 (2011).

[36] J. M. Leaf, A. Stannard, S. P. Jarvis, P. Moriarty, and J. L. Dunn (unpublished).

[37] Z. Sun, M. P. Boneschanscher, I. Swart, D. Vanmaekelbergh, and P. Liljeroth, Phys. Rev. Lett. **106**, 046104 (2011).

[38] N. Hauptmann, F. Mohn, L. Gross, G. Meyer, T. Frederiksen, and R. Berndt, New J. Phys. **14**, 073032 (2012).

[39] L. A. Girifalco, J. Phys. Chem. **95**, 5370 (1991).

[40] The error in force is estimated from the uncertainty in the oscillation amplitude, which dominates other potential sources of error.

[41] A. M. Sweetman, M. A. Rashid, S. P. Jarvis, J. L. Dunn, P. Rahe, and P. Moriarty (unpublished).

[42] Leo Gross, private communication (June 2015).